To appear in:

Journal of Theoretical and Applied Physics

Online ISSN: 2251-7235 **Print ISSN: 2251-7227**

Received: 24 December 2025

Revised: 20 January 2026

Accepted: 19 March 2026

DOI: 10.57647/jtap.2026.2004.02

Research Article

Effect of Electrode Surface Roughness on Copper Oxide Nanoparticle Synthesis via Atmospheric-Pressure Plasma in Liquid

Z. Dehghani

Plasma and Nuclear Fusion Research School, Nuclear Science and Technology Research Institute, Tehran, Iran

***Corresponding author:** dehghanyz93@gmail.com

ORCID: https://orcid.org/0009-0009-9299-0331

Abstract

Atmospheric-pressure plasma–liquid interactions provide a non-equilibrium environment for surface modification and nanostructure formation under ambient conditions. In this work, the effect of copper surface roughness on copper oxide nanostructure formation is investigated using an atmospheric-pressure plasma-in-liquid configuration in a strongly alkaline electrolyte (3 M NaOH). Copper electrodes with three controlled roughness levels were exposed to stable argon microplasma under identical operating conditions.

X-ray diffraction indicates the formation of crystalline copper oxide on the copper surface without the use of metal salt precursors. UV–Vis spectroscopy reveals optical features characteristic of copper oxide nanostructures. Electron microscopy shows a clear roughness-dependent morphological evolution, where coarse surfaces promote localized growth and agglomeration, while smoother surfaces lead to higher nucleation density and finer, more

uniform nanostructures. Elemental analysis indicates copper and oxygen as the dominant constituents of the formed layers.

The results demonstrate that surface roughness governs local electric field distribution and microdischarge interaction at the plasma–liquid interface, thereby controlling the balance between nucleation and growth. These findings highlight surface roughness as an effective parameter for tuning plasma–liquid-driven oxidation processes and contribute to a deeper understanding of plasma–liquid interaction mechanisms.

Keywords: Atmospheric-pressure plasma, Plasma–liquid interaction, Copper oxide nanostructures, Surface roughness

1- Introduction

Plasma–liquid interactions have emerged as a powerful platform for driving chemical reactions under highly non-equilibrium conditions, attracting increasing attention in plasma chemistry, materials science, and electrochemistry [1–3]. When plasma is generated in contact with or in close proximity to liquid, energetic electrons, excited species, photons, and strong electric fields interact with the liquid surface, creating a chemically active interfacial region [1, 4]. In this region, plasma-induced processes such as electron solvation, molecular dissociation, and radical formation occur simultaneously, giving rise to reaction pathways that differ fundamentally from those in conventional thermal or electrochemical systems [2, 5]. As a result, plasma–liquid systems have been explored for a wide range of applications, including water treatment, chemical synthesis, surface modification, nanomaterial fabrication, and biomedical processing [3, 6–8].

A defining feature of plasma–liquid systems is their ability to generate both oxidizing and reducing species in situ. Depending on discharge configuration and liquid chemistry, reactive species such as solvated electrons, hydrogen radicals, hydroxyl radicals, and hydrogen peroxide can be produced near the plasma–liquid interface [1,3,9]. These species enable rapid redox reactions under ambient conditions and make plasma–liquid systems particularly attractive for nanomaterial synthesis, where control over nucleation and growth is critical [4,6,10,11].

Among plasma–liquid configurations, atmospheric-pressure plasma systems are especially attractive because they operate under ambient conditions without vacuum infrastructure [3,12–14]. In these systems, the plasma may directly interact with the liquid surface or function as an electrode in a hybrid plasma–electrochemical configuration, with the plasma–liquid interface playing a central role in determining reaction pathways and interfacial chemistry [1,2].

A related class of systems is contact glow discharge electrolysis (CGDE), in which plasma forms at the interface between a metal electrode and an electrolyte under high applied voltage [15,16]. In such systems, plasma formation introduces non-Faradaic effects and localized energy deposition that can significantly influence surface modification and oxide formation on metallic electrodes [16–18]. Although atmospheric-pressure plasma–liquid systems differ from classical CGDE in geometry and discharge characteristics, both involve strong coupling between electric fields, interfacial plasma chemistry, and electrochemical reactions at metal surfaces.

Plasma–liquid interaction has therefore become an important route for the synthesis of metal and metal oxide nanomaterials. Compared to conventional wet-chemical approaches, plasma-assisted synthesis can reduce or eliminate the need for chemical reducing agents, surfactants, or high-temperature post-treatment steps [6, 11, 19]. Numerous studies have demonstrated the formation of nanoparticles and nanostructured films of noble metals, transition metals, and metal oxides using plasma interacting with liquids [11, 20–22]. However, despite this progress, achieving reproducible control over particle size, morphology, and phase composition remains a major challenge due to the complex coupling between plasma physics and liquid-phase chemistry [1, 4].

Copper and its oxides are particularly important material systems accessible through plasma–liquid synthesis. Copper oxide materials, including cuprous oxide (Cu_2O) and cupric oxide (CuO), are widely investigated for applications in catalysis, electrochemical energy conversion, sensing, and optoelectronics [23–26]. Their physical and chemical properties strongly depend on crystal structure, oxidation state, and morphology, with nanostructured and porous forms offering enhanced surface-related functionalities [24,27]. Plasma-based methods have demonstrated the formation of copper and copper oxide nanostructures in liquid environments without the use of metal salt precursors, where copper is supplied directly from the electrode and oxidized by plasma-generated reactive species [21,22, 28–30].

Liquid chemistry plays a decisive role in determining the dominant copper species formed during plasma treatment. In alkaline electrolytes, copper readily forms hydroxide and oxide species, while hydroxyl ions stabilize intermediate copper hydroxide complexes [31]. Plasma-generated oxidants such as •OH radicals and H_2O_2 further promote oxidation and dehydration reactions, often favoring CuO formation under sufficiently oxidative conditions [9, 32]. This chemical environment makes alkaline plasma–liquid systems particularly suitable for isolating surface-related effects on oxidation behavior.

In addition to plasma parameters and liquid composition, the physical state of the metal electrode itself can significantly influence plasma–liquid interactions. In electrochemical systems, surface roughness affects local current density, nucleation overpotential, and reaction kinetics. In plasma-assisted electrochemical and plasma electrolytic oxidation processes, surface roughness has been shown to influence discharge ignition, microdischarge localization, and coating morphology [33–35]. Surface asperities enhance local electric fields, promoting preferential discharge attachment and localized energy deposition. These effects can directly impact nucleation density and growth behavior during oxide formation.

Despite this recognition, the role of initial surface roughness has received limited attention in atmospheric-pressure plasma-in-liquid synthesis of copper oxide nanostructures. Many studies focus primarily on plasma parameters or electrolyte chemistry, while treating the metal electrode as a nominally uniform surface. However, when copper acts simultaneously as the reactant source and the growth substrate, surface roughness is expected to play a central role in governing copper dissolution, oxidation kinetics, and spatial distribution of plasma-induced reactions.

In strongly alkaline systems, such as NaOH electrolytes, these effects may be further amplified. High conductivity supports stable discharge operation, while hydroxyl-rich chemistry favors oxide formation [16, 31]. Localized microdischarges and enhanced electric fields at surface asperities can therefore lead to roughness-dependent differences in nucleation density, particle size, and agglomeration behavior. Understanding these effects is important both from a fundamental plasma–liquid chemistry perspective and for practical applications, since surface roughness can be readily controlled through simple mechanical pretreatment.

In this work, the effect of initial copper surface roughness on the formation of copper oxide nanostructures is systematically investigated using an atmospheric-pressure plasma-in-liquid process in a strongly alkaline electrolyte (3 M NaOH). Copper electrodes with three controlled

roughness levels, prepared by abrasive polishing, are exposed to plasma under identical operating conditions. The nanostructured oxide layers formed directly on the copper surface are characterized by X-ray diffraction, electron microscopy, energy-dispersive X-ray spectroscopy, and UV–Vis spectroscopy.

By correlating structural and compositional characteristics with the initial surface roughness, this study aims to clarify the role of surface microtexture in governing plasma–liquid-driven oxidation, nucleation, and growth behavior. The focus is placed on elucidating roughness-dependent formation mechanisms rather than establishing detailed structure–property correlations.

Unlike most plasma–liquid studies that primarily emphasize plasma parameters or electrolyte chemistry, the present work isolates surface roughness as a key physical parameter while keeping all plasma and electrolyte conditions constant. By employing a simple alkaline electrolyte without metal salt precursors, copper oxide nanostructures are generated directly from the copper electrode, enabling the intrinsic influence of surface microtexture on plasma–liquid interaction and oxide formation to be directly assessed.

2- Materials and Methods

2-1- Materials and electrolyte preparation

Copper sheets with a purity of 99.5% and a thickness of 0.8 mm were used as the copper electrode (substrate/anode). Silicon carbide (SiC) abrasive papers with grit sizes of 400, 600, and 1200 were employed to prepare copper surfaces with different roughness levels.

The electrolyte consisted of deionized water and 3 M sodium hydroxide (NaOH) solution (40 mL). No additional metal precursors or silver-containing compounds were added to the electrolyte. All chemicals were of analytical grade and used without further purification.

2-2- Preparation of copper electrodes with controlled surface roughness

Copper sheets were cut into identical specimens with a geometric area of 2 cm^2. The samples were mechanically polished using SiC abrasive papers with grit sizes of 400, 600, and 1200 to obtain different surface roughness levels, followed by ultrasonic cleaning in acetone, ethanol, and deionized water. Polishing was performed under identical conditions for all samples to

ensure reproducibility. After polishing, the samples were ultrasonically cleaned to remove residual contaminants and then dried at room temperature prior to plasma treatment.

The color change of the electrolyte during plasma treatment is reported as a qualitative indication of copper-related species generated through plasma–liquid interaction. No quantitative solution-phase analysis was performed; therefore, the exact identity and concentration of dissolved copper species could not be determined.

In strongly alkaline solutions, dissolved copper is commonly stabilized as Cu(II) hydroxo complexes, which likely contribute to the observed blue–green coloration of the electrolyte during plasma exposure.

Surface roughness in this study is treated as a relative parameter defined by standardized abrasive paper grades rather than absolute numerical values. The use of SiC papers provides reproducible and monotonic variations in surface microtexture, which are sufficient for comparative analysis of roughness-dependent plasma–liquid interaction effects. Quantitative roughness measurements (e.g., Ra or RMS) were not performed and are identified as an important direction for future work.

2-3- Plasma-in-liquid reactor configuration

Atmospheric-pressure microplasma was generated using a DC high-voltage power supply in a plasma–liquid interaction configuration. A stainless-steel hollow needle served as the cathode and was positioned 2 mm above the liquid surface, while the polished copper sheet was immersed in the electrolyte and acted simultaneously as the anode and substrate for nanostructure formation.

Argon gas was supplied through the hollow cathode at a flow rate of 250 sccm to sustain a stable discharge. The plasma was operated in constant-current mode at 5 mA using a 100 kΩ ballast resistor connected in series with the power supply to ensure discharge stability. Voltage and current were continuously monitored during plasma operation.

No plasma diagnostic measurements (e.g., electron temperature or optical emission spectroscopy) were performed in this study. All plasma operating conditions were kept identical for all experiments in order to isolate the effect of surface roughness on plasma–liquid-driven nanostructure formation.

2-4- Plasma-assisted synthesis procedure

For each experiment, a fixed volume of the electrolyte was placed in a glass reactor, and a copper sample (R400, R600, or R1200) was vertically immersed at a fixed position to ensure consistent discharge geometry across experiments. After establishing the argon flow, the plasma discharge was ignited above the electrolyte surface and maintained for 20 min for all samples under identical operating conditions.

All plasma treatments were repeated multiple times for each surface roughness condition (R400, R600, and R1200) to confirm experimental reproducibility. No plasma-off or electrolyte-only control experiments were performed. All experiments were conducted under identical plasma and electrolyte conditions to isolate the effect of surface roughness.

2-5- Post-treatment procedure

After 20 min of plasma treatment, the discharge was switched off and the copper substrate was removed from the electrolyte. The treated copper sheets were rinsed thoroughly with deionized water to remove weakly adhered residues and then washed with ethanol. The samples were subsequently dried in an oven at 80 °C for 1 h before characterization.

No nanoparticles were collected from the liquid phase. All structural and phase analyses were performed on the material formed directly on the copper substrate surface after plasma treatment.

2-6- Characterization techniques

The surface morphology of the copper electrodes before and after plasma treatment was examined using field-emission scanning electron microscopy (FESEM). Images were acquired from multiple regions of each sample to assess surface texture, nanostructure formation, roughness-dependent morphological features, and spatial uniformity across the R400, R600, and R1200 samples.

Elemental composition of the plasma-treated surfaces was analyzed by energy-dispersive X-ray spectroscopy (EDS) attached to the FESEM system to confirm the presence of copper-based nanostructures and oxygen incorporation resulting from plasma–liquid interactions. It should be noted that EDS provides qualitative elemental information and does not allow determination of copper oxidation states.

Phase identification of the nanostructured layers formed directly on the copper substrates was performed using X-ray diffraction (XRD) with a Philips X'Pert MPD diffractometer employing

Co Kα radiation (λ = 1.79 Å). The diffraction patterns were recorded over an appropriate 2θ range to identify crystalline copper and copper oxide phases formed during plasma processing.

UV–Vis spectroscopy was employed as a representative technique to confirm the presence of copper oxide–related optical features after plasma treatment. A systematic comparison among different surface roughness conditions was not pursued, as the oxide layers were formed on opaque copper substrates and the measured optical response can be strongly influenced by roughness-dependent scattering and reflectance effects. A more rigorous roughness-dependent optical analysis would require diffuse reflectance spectroscopy with an integrating sphere or other specialized optical methods.

3- Results and Discussion

3-1- Observation of plasma–liquid interaction and solution evolution

Figure 1 shows photographs of the experimental setup and the electrolyte solution after 20 min of atmospheric-pressure plasma treatment. During plasma operation, intensive bubble formation was observed at the plasma–liquid interface and near the copper electrode surface, indicating active plasma–liquid interactions and electrochemical reactions. The generation of gas bubbles can be attributed to plasma-induced decomposition of water molecules and electrochemical reactions occurring at the copper electrode.

Figure 1. Photographs of the atmospheric-pressure plasma-in-liquid (APPL) experiment using a polished copper electrode (R600) immersed in alkaline electrolyte:

After plasma exposure, the initially transparent solution exhibited a distinct color change to a greenish/blue-green appearance (Figure 1), suggesting the formation of copper-based species in the solution and/or on the electrode surface. Such color evolution is commonly associated

with the presence of Cu^{2+} complexes and copper oxide/hydroxide nanostructures generated through plasma-assisted redox reactions.

The strong interaction between the plasma discharge and the copper electrode promotes localized heating, enhanced electric field concentration, and the generation of highly reactive species (e.g., solvated electrons, •OH radicals), which collectively facilitate surface modification and nanostructure formation on the copper substrate.

3-2- UV–Vis absorption analysis

The UV–Vis absorption spectrum of the plasma-treated sample is presented in Figure 2, recorded in the wavelength range of 200–800 nm. A strong absorption band is observed in the ultraviolet region below approximately 300 nm, which can be attributed to charge-transfer transitions and interband transitions in copper oxide species.

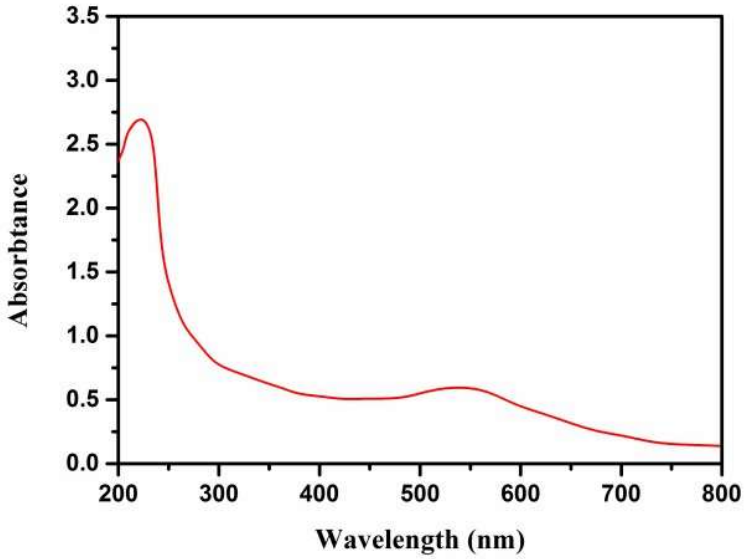

Figure 2. UV–Vis absorption spectrum of the sample obtained after 20 min of atmospheric-pressure plasma treatment using the R600 copper electrode in alkaline electrolyte

In addition, a broad absorption feature centered on the visible region (approximately 500–600 nm) is detected. This absorption band is commonly associated with copper oxide (CuO/Cu_2O) nanostructures and can be linked to d–d electronic transitions and defect-related states in copper oxide nanoparticles. The broad nature of the absorption band suggests a distribution of particle sizes and possible coexistence of multiple copper oxide phases. UV–Vis analysis was

performed on a representative sample (R600) to confirm copper oxide formation, while roughness-dependent effects were primarily evaluated based on FESEM morphology.

The absence of a sharp and well-defined surface plasmon resonance (SPR) peak characteristic of metallic copper nanoparticles (typically reported around 560–580 nm) indicates that the dominant species formed under the present plasma conditions are copper oxide nanostructures rather than pure metallic Cu nanoparticles. This observation is consistent with the oxidative plasma environment and the presence of reactive oxygen species generated during plasma–liquid interaction.

Accordingly, UV–Vis results are presented as representative confirmation of copper oxide formation, while roughness-dependent effects discussed in this work are primarily limited to morphological evolution rather than optical property modulation.

3-3- X-ray diffraction (XRD) analysis

Figure 3 shows the XRD pattern obtained from the material formed directly on the copper electrode surface after 20 min of plasma treatment. The diffraction peaks observed at $2\theta \approx 32.5°$, 35.5°, and 38.7° can be indexed to the (110), (−111), and (111) crystallographic planes of monoclinic CuO, respectively, in good agreement with the standard reference data (JCPDS card No. 45-0937). The presence of these well-defined reflections confirms the formation of crystalline CuO during plasma treatment.

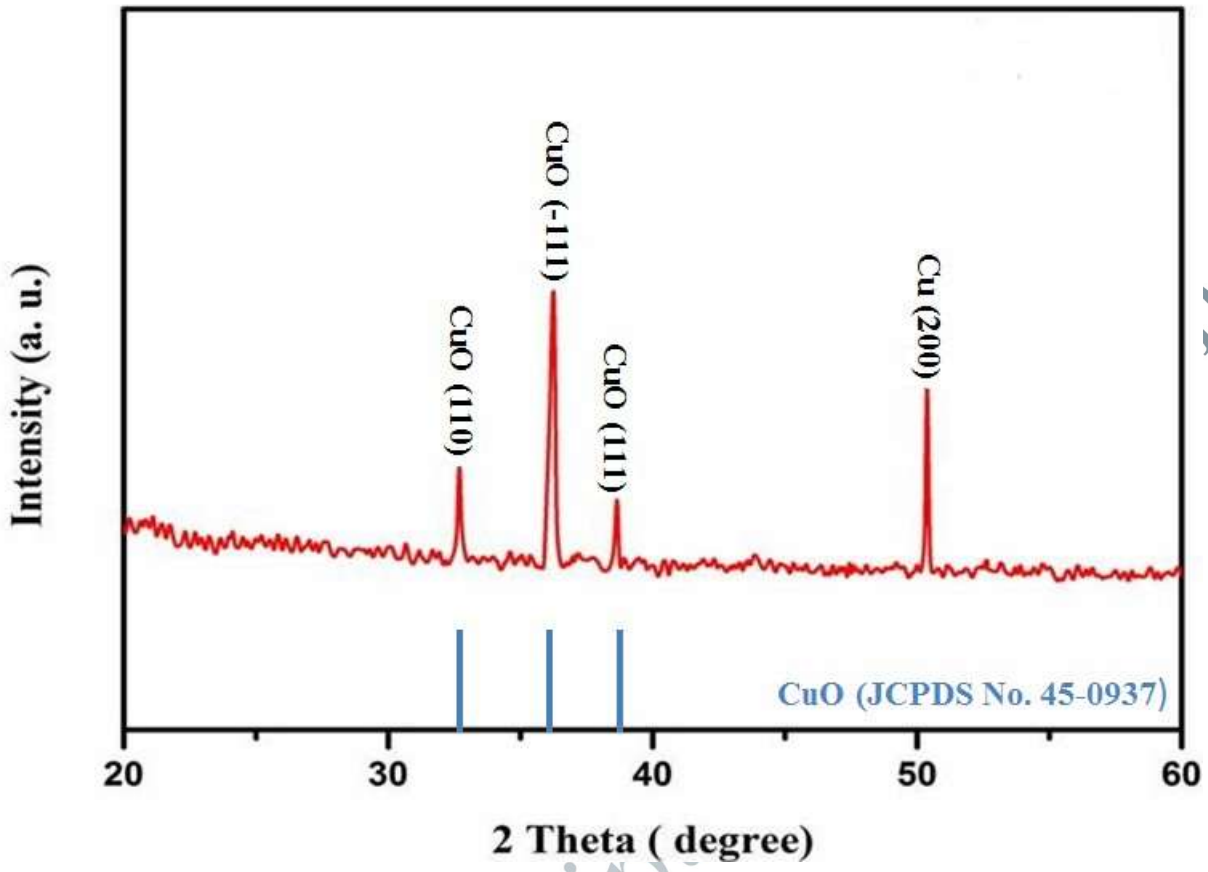

Figure 3 X-ray diffraction (XRD) pattern of the plasma-treated R600 copper electrode. The peaks at 2θ ≈ 32.5°, 35.5°, and 38.7° are indexed to monoclinic CuO (JCPDS card No. 45-0937), while the intense peak near 50–52° originates from the metallic copper substrate.

A strong diffraction peak observed near 2θ ≈ 50–52° is attributed to metallic Cu originating from the underlying copper substrate and is therefore not assigned to copper oxide phases.

Importantly, no characteristic diffraction peaks corresponding to cuprous oxide (Cu_2O), such as the (111) reflection at ~36.4° or the (200) reflection at ~42.3° (for Cu Kα radiation), were detected within the sensitivity limits of the measurement. This absence, together with the clear presence of CuO reflections, indicates that CuO is the dominant crystalline phase formed under the present plasma–liquid interaction conditions.

The preferential formation of CuO can be attributed to the strongly alkaline electrolyte (3 M NaOH) and the highly oxidative plasma environment, where reactive oxygen species (e.g., •OH radicals and H_2O_2) promote the oxidation of Cu(I) intermediates to Cu(II) oxide. Although the presence of minor amorphous phases or sub-detectable Cu_2O fractions cannot be completely excluded, the combined XRD, UV–Vis, and EDS results consistently support CuO as the dominant phase.

3-4- Correlation between optical and structural results

The UV–Vis and XRD results are in good agreement and collectively confirm the formation of copper oxide nanostructures during plasma treatment. The broad visible absorption band observed in the UV–Vis spectrum corresponds well with the crystalline CuO phase identified by XRD analysis. This consistency indicates that the optical response of the sample is dominated by copper oxide rather than metallic copper nanoparticles.

The combined results demonstrate that atmospheric-pressure plasma in a electrolyte provides a rapid and effective route for the formation of crystalline copper oxide nanostructures directly on a copper substrate without the need for additional chemical reducing or oxidizing agents.

3-5- Effect of surface roughness on surface morphology

Accordingly, the discussion focuses on comparative morphological trends associated with different surface roughness classes (R400, R600, and R1200) rather than absolute roughness values. Figure 4 presents FESEM images of copper electrode surfaces with different initial roughness levels after 20 min of atmospheric-pressure plasma treatment in alkaline electrolyte.

.

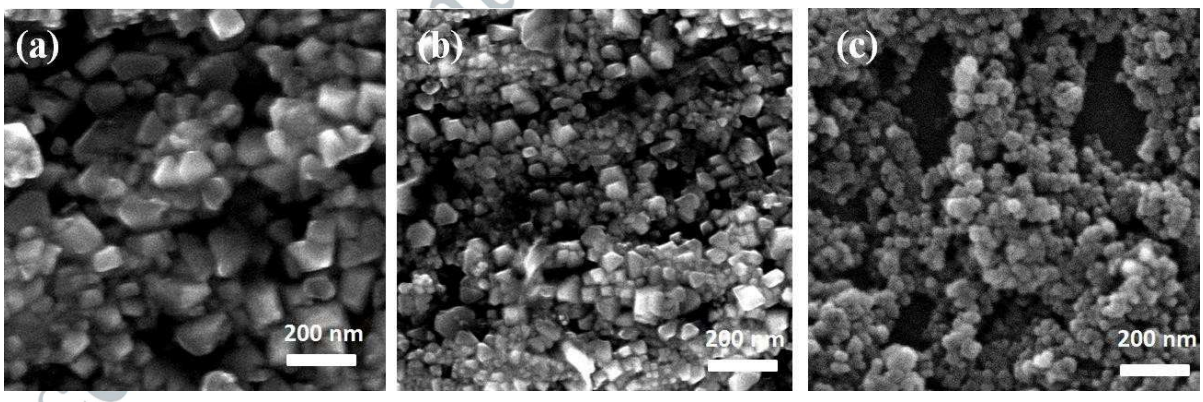

Figure 4. FESEM images of nanostructured layers formed on copper electrodes with different initial surface roughness after **20 min** of atmospheric-pressure plasma treatment in alkaline electrolyte (40 mL deionized water and 3 M NaOH): (a) R400 (coarse surface), (b) R600 (medium roughness), and (c) R1200 (fine surface).

As shown in Figure 4a, the R400 sample exhibits relatively large, faceted nanostructures with irregular shapes and a non-uniform size distribution. These structures are densely packed and

form agglomerated clusters with limited interparticle spacing. The coarse initial surface roughness introduces pronounced surface asperities that enhance localized plasma–electrode interactions, promoting particle coalescence and growth into larger crystallites.

In contrast, the R600 surface shown in Figure 4b displays a more homogeneous and uniformly distributed nanostructure morphology. The nanostructures are smaller and more regularly shaped compared to R400, with improved surface coverage and reduced agglomeration. This suggests that an intermediate surface roughness provides a balance between nucleation density and growth, allowing plasma-induced species to interact more evenly across the surface.

For the R1200 sample (Figure 4c), a high density of fine nanostructures with significantly smaller particle size and a more porous morphology is observed. The smoother initial surface promotes more uniformly distributed nucleation sites while limiting localized growth, resulting in finer nanostructures and increased porosity.

Overall, the FESEM observations in Figure 4 demonstrate that increasing the polishing grade from R400 to R1200 shifts the dominant behavior from particle growth and agglomeration toward enhanced nucleation and size refinement. Although absolute roughness parameters were not quantified, the use of standardized abrasive papers enables reliable comparative assessment of roughness-dependent effects.

The morphological trends shown in Figure 4 were consistently reproduced across multiple samples and surface regions, indicating good experimental reproducibility. The morphological analysis presented here is therefore intended as a comparative, trend-based evaluation rather than a fully quantitative particle size analysis. Due to the heterogeneous and agglomerated nature of the plasma-formed oxide structures, automated extraction of particle size distributions was not pursued, and terms such as nucleation density and growth are used qualitatively to describe relative morphological features observed in the FESEM images.

To further support the qualitative morphological observations, particle size distribution histograms were extracted from the FESEM images for all three surface roughness conditions. As shown in Figure 5, at least 20 individual particles were analyzed for each sample. The resulting histograms confirm that the R400 surface exhibits larger particle sizes with broader dispersion, whereas the R600 and R1200 surfaces show smaller and more narrowly distributed particle sizes, consistent with the observed roughness-dependent nucleation and growth behavior.

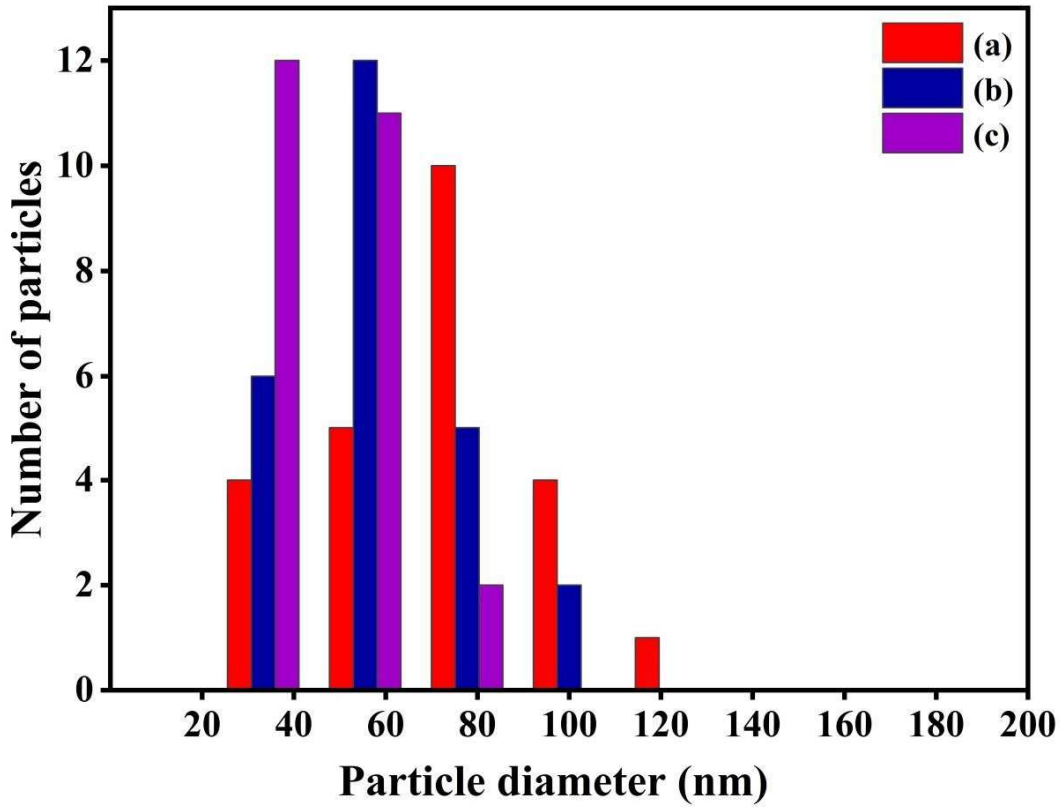

Figure 5. Particle size distribution histograms derived from FESEM images for copper oxide nanostructures formed on copper electrodes with different surface roughness: (a) R400, (b) R600, and (c) R1200. At least 20 particles were analyzed for each sample.

3-6- Elemental composition analysis (EDS)

The elemental composition of the plasma-treated copper surface was analyzed by energy-dispersive X-ray spectroscopy (EDS), as shown in Figure 6. The EDS spectrum exhibits strong characteristic peaks corresponding to Cu along with a clear O signal, indicating the formation of copper oxide–based nanostructures on the electrode surface.

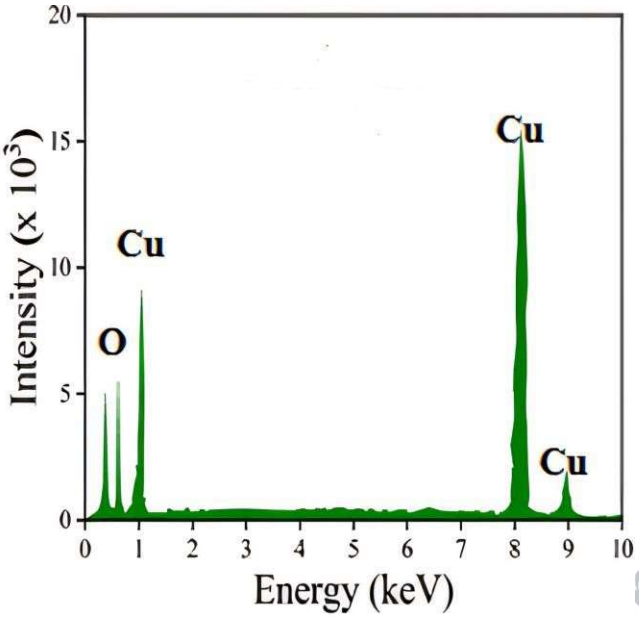

Figure 6. Energy-dispersive X-ray spectroscopy (EDS) spectrum acquired from the plasma-treated copper surface, confirming the presence of copper and oxygen as the dominant elements in the nanostructured layer formed during plasma processing.

As illustrated in Figure 6, no additional impurity-related peaks are detected within the sensitivity limits of the EDS technique, suggesting that the nanostructured layer consists primarily of copper and oxygen. The presence of oxygen can be attributed to the highly oxidative plasma–liquid environment in the alkaline electrolyte, where reactive oxygen species (e.g., •OH radicals and dissolved oxygen) promote oxidation of copper atoms released from the electrode surface.

The EDS results shown in Figure 6 are consistent with the XRD analysis, which identified crystalline CuO as the dominant phase, and with the UV–Vis absorption features characteristic of copper oxide nanostructures. Together with FESEM observations, these results indicate that surface roughness influences not only the morphology but also the effective oxidation behavior during plasma-assisted synthesis. The roughness-dependent morphological evolution is attributed to variations in local electric field concentration at surface asperities, where coarser surfaces (R400) enhance microdischarge localization and particle growth, while smoother surfaces (R1200) promote higher nucleation density and finer nanostructures.

It should be noted that EDS provides qualitative elemental information only and cannot distinguish between copper oxidation states or determine oxide stoichiometry. Therefore, the identification of copper oxide formation in this study is based on complementary evidence from

XRD phase analysis, UV–Vis spectroscopy, and the strongly oxidative alkaline plasma environment. The absence of impurity-related peaks in Figure 6 does not imply chemical purity but indicates that no major foreign elements were introduced during plasma processing within the detection limits of the technique.

4- Mechanism of copper oxide nanostructure formation

The following mechanism is proposed as a qualitative and phenomenological interpretation based on experimental observations and established plasma–liquid interaction literature. While purely chemical oxidation of copper in alkaline environments is possible, it is generally slow and does not typically produce the highly localized and roughness-dependent nanostructures observed here within short treatment times. The rapid formation of nanostructured CuO layers, together with intensive gas evolution and localized surface modification, strongly suggests a dominant contribution from plasma–liquid interactions.

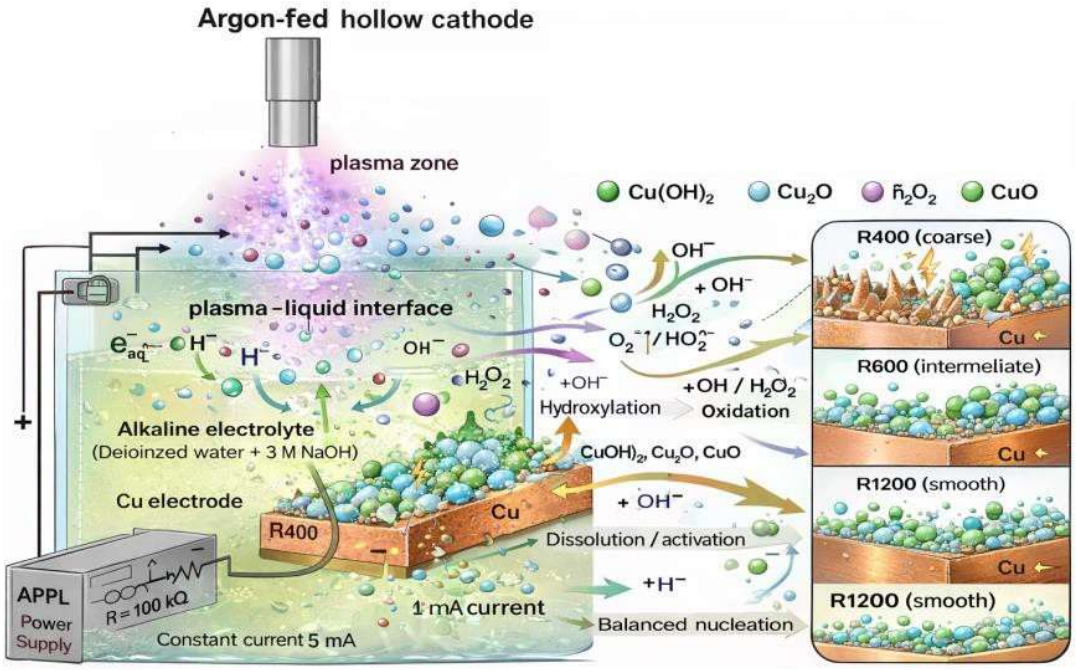

Figure 7. Schematic illustration of the atmospheric-pressure plasma-in-liquid process and the proposed roughness-dependent formation mechanism of copper oxide nanostructures on copper electrodes in alkaline electrolyte (3 M NaOH).

As schematically illustrated in Figure 7, the atmospheric-pressure plasma-in-liquid process initiates with the generation of a non-thermal microplasma above the alkaline electrolyte surface. The argon-fed hollow cathode produces a stable discharge that interacts with the liquid surface, forming an active plasma–liquid interface. At this interface, energetic electrons and excited species transfer energy into the liquid phase, leading to the formation of reactive species such as solvated electrons, hydrogen radicals, hydroxyl radicals, atomic oxygen, and hydrogen peroxide. These species subsequently diffuse from the interface into the bulk electrolyte and toward the copper electrode.

In the strongly alkaline environment provided by the 3 M NaOH electrolyte, the copper electrode undergoes surface activation under the combined influence of the applied electric field and plasma-generated reactive species. Copper atoms at the surface are oxidized and interact with hydroxide ions to form copper hydroxide intermediates, which are subsequently transformed into copper oxide phases through oxidation and dehydration reactions promoted by reactive oxygen species such as •OH and H_2O_2. As a result, nucleation of copper oxide species occurs directly on the copper substrate, followed by growth into a nanostructured oxide layer during plasma exposure.

The initial surface roughness of the copper electrode strongly influences the local electric field distribution and the interaction between the plasma and the electrode surface. For coarse surfaces (R400), sharp surface asperities enhance local electric field intensity and promote localized energy deposition and microdischarge interactions, favoring rapid growth and agglomeration of oxide nuclei into larger and less uniform nanostructures. In contrast, smoother surfaces (R1200) distribute the electric field more uniformly, increasing the density of nucleation sites while limiting localized overheating, which results in finer and more uniformly distributed nanostructures. The intermediate roughness condition (R600) represents a balanced regime in which nucleation and growth processes occur more uniformly, leading to a homogeneous nanostructured surface with moderate particle size.

The discussion of nucleation and growth behavior presented here is intended as a phenomenological interpretation based on final-state morphology rather than a kinetic description derived from time-resolved measurements.

Overall, the schematic shown in Figure 7 highlights the synergistic roles of plasma-generated reactive species, alkaline electrolyte chemistry, and surface roughness in governing the nucleation and growth of copper oxide nanostructures. Roughness-dependent electric field localization controls the balance between nucleation and growth, thereby determining the final morphology and spatial distribution of the oxide nanostructured layer formed on the copper electrode. The proposed reaction pathways are consistent with the observed phase composition, morphology, and electrolyte conditions, although transient intermediate species and time-dependent evolution were not directly probed in the present study.

Compared to conventional electrochemical oxidation and classical contact glow discharge electrolysis, the present atmospheric-pressure plasma–liquid configuration enables non-equilibrium plasma chemistry under ambient conditions without the use of salt precursors. Unlike many plasma–liquid studies that emphasize discharge parameter tuning, the present results demonstrate that surface roughness alone can serve as an effective control parameter for nanostructure formation, highlighting an often-overlooked aspect of plasma–metal–liquid interactions.

5-Conclusion

In this study, copper oxide nanostructures were successfully formed directly on copper electrodes using an atmospheric-pressure plasma-in-liquid process in a strongly alkaline electrolyte without the use of metal salt precursors. By systematically varying the initial surface roughness while maintaining identical plasma and electrolyte conditions, the role of surface microtexture in plasma–liquid-driven oxidation and nanostructure formation was isolated and clarified. Structural and compositional analyses confirm copper oxide as the dominant phase formed under the present plasma conditions. FESEM observations reveal a clear roughness-dependent evolution of surface morphology, where coarser surfaces promote localized growth and agglomeration of oxide structures, while smoother surfaces favor higher apparent nucleation density and the formation of finer, more uniformly distributed nanostructures. These trends are supported by EDS results confirming copper and oxygen as the primary constituents of the plasma-formed layers.

The observed roughness-dependent behavior is attributed to differences in local electric field enhancement and microdischarge interaction at the plasma–liquid interface, which govern the balance between nucleation and growth processes in the alkaline environment. The proposed

formation mechanism is qualitative and phenomenological, intended to rationalize the experimentally observed trends based on established plasma–liquid interaction principles rather than to provide a detailed kinetic description.The novelty of this work lies in demonstrating that initial surface roughness, independent of plasma operating conditions and electrolyte chemistry, can serve as a simple and effective physical control parameter for tailoring copper oxide nanostructures in atmospheric-pressure plasma–liquid systems. This finding highlights the importance of the metal surface state in plasma-assisted oxidation processes, an aspect that is often overlooked in plasma–liquid studies focused primarily on discharge or solution parameters.

Future work will focus on incorporating quantitative surface roughness measurements (e.g., profilometry or atomic force microscopy), surface-sensitive chemical analysis techniques (such as XPS and Raman spectroscopy), and time-resolved plasma diagnostics to establish more detailed correlations between roughness parameters, plasma-induced reaction pathways, and nanostructure evolution. The insights gained in this study contribute to a deeper understanding of plasma–liquid interactions at reactive metal surfaces and support the development of controllable and scalable plasma-based approaches for oxide nanostructure fabrication.

References

1. Bruggeman, P. J., Kushner, M. J., Locke, B. R., Gardeniers, J. G. E., Graham, W. G., Graves, D. B., … Bogaerts, A. (2016). Plasma–liquid interactions: A review and roadmap. *Plasma Sources Science and Technology, 25*(5), 053002. https://doi.org/10.1088/0963-0252/25/5/053002

2. Mariotti, D., & Sankaran, R. M. (2010). Microplasmas for nanomaterials synthesis. *Journal of Physics D: Applied Physics, 43*(32), 323001. https://doi.org/10.1088/0022-3727/43/32/323001

3. Mariotti, D., Patel, J., Švrček, V., & Maguire, P. (2012). Plasma–liquid interactions at atmospheric pressure for nanomaterials synthesis and surface engineering. *Plasma Processes and Polymers, 9*(11–12), 1074–1085. https://doi.org/10.1002/ppap.201200080

4. Locke, B. R., Sato, M., Sunka, P., Hoffmann, M. R., & Chang, J.-S. (2006). Electrohydraulic discharge and nonthermal plasma for water treatment. *Industrial & Engineering Chemistry Research, 45*(3), 882–905. https://doi.org/10.1021/ie050981u

5. Rezaei, F., Vanraes, P., Nikiforov, A. Y., & Leys, C. (2019). Applications of plasma–liquid systems: A review. *Materials, 12*(17), 2751. https://doi.org/10.3390/ma12172751

6. Saito, G., & Akiyama, T. (2015). Nanomaterial synthesis using plasma generation in liquid. *Journal of Nanomaterials, 2015*, 123696. https://doi.org/10.1155/2015/123696

7. Bruggeman, P., & Leys, C. (2009). Non-thermal plasmas in and in contact with liquids. *Journal of Physics D: Applied Physics, 42*(5), 053001. https://doi.org/10.1088/0022-3727/42/5/053001

8. Shirai, N., Uchida, S., & Tochikubo, F. (2014). Chemical reactions in liquid induced by atmospheric-pressure glow discharge with liquid electrode. *Plasma Sources Science and Technology, 23*(5), 054006. https://doi.org/10.1088/0963-0252/23/5/054006

9. Mun, M. K., Li, Y., & Sankaran, R. M. (2017). Solution plasma synthesis of nanoparticles. *Journal of Physics D: Applied Physics, 50*(27), 273002. https://doi.org/10.1088/1361-6463/aa74d8

10. Lin, L., & Keidar, M. (2015). Microplasmas: Technology and applications. *Journal of Applied Physics, 118*(3), 033301. https://doi.org/10.1063/1.4926866

11. Greda, K., Jamroz, P., Pohl, P., & Zyrnicki, W. (2016). Flowing liquid anode atmospheric pressure glow discharge. *Analytical Chemistry, 88*(15), 7476–7485. https://doi.org/10.1021/acs.analchem.6b01709

12. Jiang, B., Zheng, J., Qiu, S., Wu, M., Zhang, Q., Yan, Z., & Xue, Q. (2014). Review on electrical discharge plasma technology for wastewater remediation. *Chemical Engineering Journal, 236*, 348–368. https://doi.org/10.1016/j.cej.2013.09.090

13. Hickling, A., & Ingram, M. D. (1964). Glow-discharge electrolysis. *Journal of Electroanalytical Chemistry, 8*(1), 65–81. https://doi.org/10.1016/0022-0728(64)80012-1

14. Gupta, S. K. (2015). Contact glow discharge electrolysis: Its origin, plasma diagnostics and non-faradaic chemical effects. *Journal of Physics D: Applied Physics, 48*(42), 425201. https://doi.org/10.1088/0022-3727/48/42/425201

15. Sunka, P. (2001). Pulse electrical discharges in water and their applications. *Physics of Plasmas, 8*(5), 2587–2594. https://doi.org/10.1063/1.1352595

16. Dufour, T., Gherardi, N., & Boutin, B. (2015). Modeling of atmospheric pressure discharges over water. *Plasma Chemistry and Plasma Processing, 35*, 117–135. https://doi.org/10.1007/s11090-014-9586-7

17. Sankaran, R. M., Holunga, D., Flagan, R. C., & Giapis, K. P. (2005). Synthesis of blue luminescent Si nanoparticles using atmospheric-pressure microdischarges. *Nano Letters, 5*(3), 537–541. https://doi.org/10.1021/nl050085b

18. Saito, G., Hosokai, S., Tsubota, M., & Akiyama, T. (2011). Synthesis of copper/copper oxide nanoparticles by solution plasma. *Journal of Applied Physics, 110*(2), 023302. https://doi.org/10.1063/1.3608240

19. Velusamy, T., La, C. H., Sankaran, R. M., & Mariotti, D. (2017). Ultra-small CuO nanoparticles synthesized by a hybrid plasma–liquid process. *Plasma Processes and Polymers, 14*(7), e1600224. https://doi.org/10.1002/ppap.201600224

20. Du, C. M., Yan, Z. G., Ren, X. D., & Wang, Y. N. (2014). Cu_2O nanoparticles synthesized by atmospheric pressure microplasma. *Scientific Reports, 4*, 7339. https://doi.org/10.1038/srep07339

21. Wang, Z., & Li, Y. (2012). Cu_2O nanostructures: Synthesis and applications. *Journal of Materials Chemistry, 22*, 16102–16111. https://doi.org/10.1039/C2JM33055K

22. Zhang, Q., Zhang, K., & Xu, D. (2014). CuO nanostructures: Synthesis, characterization, growth mechanisms, fundamental properties, and applications. *Progress in Materials Science, 60*, 208–337. https://doi.org/10.1016/j.pmatsci.2013.09.003

23. Wang, Y., Li, J., & Liu, Y. (2019). Copper oxide nanomaterials for energy and environmental applications. *Chemical Engineering Journal, 362*, 109–136. https://doi.org/10.1016/j.cej.2019.01.037

24. Liguori, A., Trisolini, E., Laurita, R., et al. (2018). Synthesis of copper-based nanostructures by non-equilibrium atmospheric pressure plasma jet in liquid. *Plasma Chemistry and Plasma Processing, 38*, 1209–1222. https://doi.org/10.1007/s11090-018-9921-4

25. Glad, X., et al. (2020). Synthesis of copper and copper oxide nanomaterials by spark discharges in liquids. *Nanomaterials, 10*(8), 1584. https://doi.org/10.3390/nano10081584

26. Galif, H., et al. (2022). Copper nanoparticles synthesized via solution plasma process. *ACS Omega, 7*(10), 8630–8639. https://doi.org/10.1021/acsomega.1c07027

27. Lu, Q., et al. (2021). Plasma-assisted synthesis of Cu_2O nanosheets in alkaline electrolyte. *Electrochimica Acta, 367*, 137483. https://doi.org/10.1016/j.electacta.2020.137483

28. Kaushik, N. K., et al. (2019). Plasma and nanomaterials: Fabrication and biomedical applications. *Nanomaterials, 9*(1), 98. https://doi.org/10.3390/nano9010098

29. Brisset, J. L., & Pawlat, J. (2016). Chemical effects of air plasma species in aqueous media. *Plasma Chemistry and Plasma Processing, 36*, 355–381. https://doi.org/10.1007/s11090-015-9707-6

30. Clyne, T. W., & Troughton, S. C. (2019). A review of recent work on discharge characteristics during plasma electrolytic oxidation. *Surface Engineering, 35*(3), 191–215. https://doi.org/10.1080/02670844.2018.1467889

31. Zhu, L., Liu, C., & Yang, S. (2017). Effect of surface roughness on plasma electrolytic oxidation coatings. *Surface and Coatings Technology, 325*, 405–413. https://doi.org/10.1016/j.surfcoat.2017.06.075

32. Dehnavi, V., Luan, B. L., Liu, X. Y., Shoesmith, D. W., & Rohani, S. (2014). Correlation between plasma discharge and coating formation. *Surface and Coatings Technology, 251*, 106–114. https://doi.org/10.1016/j.surfcoat.2014.04.036